

Cu(I)-I coordination polymers as possible substitutes of lanthanides as downshifters for increasing the conversion efficiency of solar cells.

Supporting Information

S1. Synthesis procedure.

S2. Structural characterization.

S2.1. Single crystal X-Ray diffraction (SCXRD) of compound 1D-[Cu(NH₂-MeIN)]_n.

S2.2. Powder X-ray diffraction (PXRD) analysis of compound 1D-[Cu(NH₂-MeIN)]_n and [Cu(NH₂-MeIN)]_n@EVA thin films.

S2.3. Infrared spectroscopy.

S2.4. Thermal characterization.

S2.5. Diffuse reflectance UV-visible spectroscopy.

S3. Morphological studies.

S4. Luminescent behavior.

S5. Transparency and flexibility.

S6. SEM Study

S7. Stress-Strain curves

S1. Synthesis procedure.

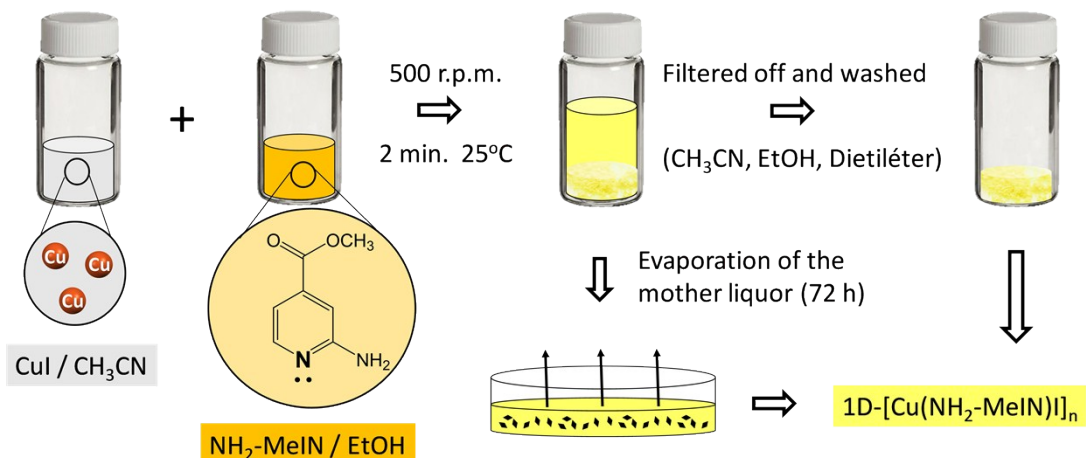


Figure S1. Schematic synthesis of compound $1D\text{-}[Cu(NH}_2\text{-MeIN})I]_n$.

S2. Structural characterization.

S2.1. Single crystal X-Ray diffraction (SCXRD) of compound 1D-[Cu(NH₂-MeIN)I]_n.

Table S1. Lattice parameters of compound 1D-[Cu(NH₂-MeIN)I]_n at 296 K (RT) and at 110 K (LT).

Compound	(1D-[Cu(NH ₂ -MeIN)I] _n) ^{RT}	(1D-[Cu(NH ₂ -MeIN)I] _n) ^{LT}
Empirical formula	C ₇ H ₈ CuIN ₂ O ₂	C ₇ H ₈ CuIN ₂ O ₂
Formula weight	342.59	300.57
T (K)	296	110
λ (Å)	0.71073	0.71073
Crystal system	Triclinic	Triclinic
Space group	<i>P</i> -1	<i>P</i> -1
a (Å)	4.2503(2)	4.2103(3)
b (Å)	10.1169(4)	9.9279(6)
c (Å)	11.3784(5)	11.2864(7)
α (°)	81.030(3)	82.189(3)
β (°)	88.843(3)	89.223(3)
γ (°)	82.580(4)	83.312(3)
V (Å ³)	479.24(4)	464.21(5)
Z	2	2
ρ _{calc} (g·cm ⁻³)	2.374	2.451
μ (mm ⁻¹)	5.467	5.644
Reflexion collected	2481	1691
Unique data /parameters	2481/127	1691/119
Goodness of fit (<i>S</i>)	1.036	1.319
<i>R</i> 1/ <i>wR</i> 2 [<i>I</i> >2σ(<i>I</i>)]	0.0247/0.0477	0.0189/0.0548
<i>R</i> 1/ <i>wR</i> 2 [all data]	0.0292/0.0493	0.0235/0.0740

Table S2. Bond distances (Å) and bond angles (°) of compound 1D-[Cu(NH₂-MeIN)I]_n at 296 K (RT) and 110 K (LT).

Compound	(1D-[Cu(NH₂-MeIN)I]_n)^{RT}	(1D-[Cu(NH₂-MeIN)I]_n)^{LT}
Cu-I1 _{rail}	2.643(2)	2.6257(6)
Cu-I1 ⁱ _{rail}	2.733(2)	2.7181(6)
Δ[Cu-I1 _{rail}]	0.090	0.0924
Cu-I1 _{rung}	2.680(2)	2.6682(6)
Cu-N1	2.04(1)	2.028(4)
Cu-Cu ⁱⁱ	2.682(4)	2.627(1)
Cu-Cu ⁱⁱⁱ	3.514	3.523
Δ[Cu-Cu]	0.832	0.896
I1-Cu1-I1 ⁱ	104.33(8)	103.96(2)
I1 ⁱ -Cu1-I1 ⁱⁱ	99.05(7)	98.31(2)
I1-Cu1-I1 ⁱⁱ	119.51(8)	120.50(2)
Cu1-I1 ⁱ -Cu1 ⁱⁱ	80.95(7)	81.69(2)
Cu1-I1-Cu1 ⁱⁱⁱ	104.34(8)	103.96(2)
Cu1 ⁱⁱ -I1-Cu1 ⁱⁱⁱ	60.49(8)	59.50(2)
Dihedral angle	112.22	111.65
Tilt angle	87.47	88.19
Twist angle	53.52	52.87

Symmetry codes: i) x-1, y, z; ii) -x, -y, -z+1; iii) -x+1, -y, -z+1

S2.2. Powder X-ray diffraction (PXRD) analysis of compound 1D-[Cu(NH₂-MeIN)I]_n and [Cu(NH₂-MeIN)I]_n@EVA thin films.

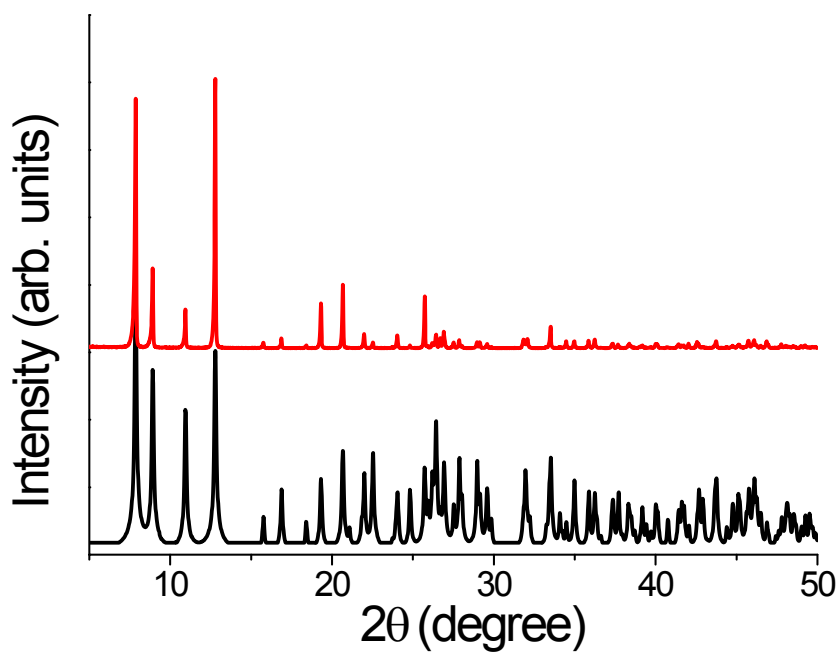


Figure S2. X-ray powder diffractogram of compound **1D-[Cu(NH₂-MeIN)]_n**: Experimental (red line) and theoretical (black line).

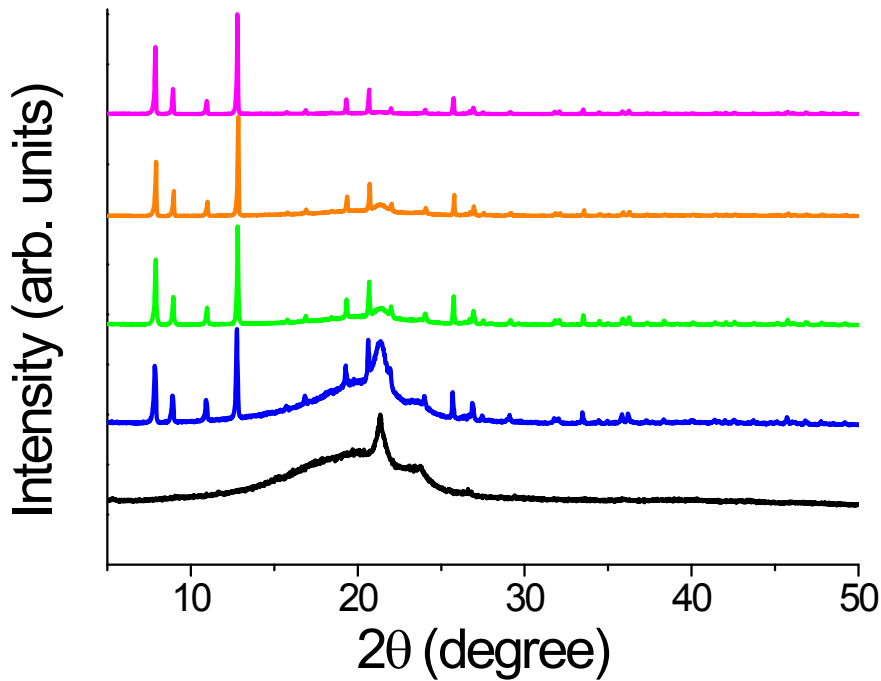


Figure S3. X-ray powder diffractogram of EVA (black line), **1D-[Cu(NH₂-MeIN)]_n** (blue line), $[Cu(NH_2-MeIN)]_n$ @EVA-5% (blue line), $[Cu(NH_2-MeIN)]_n$ @EVA-10% (green line), $[Cu(NH_2-MeIN)]_n$ @EVA-15% (orange line) and $[Cu(NH_2-MeIN)]_n$ @EVA-30% (purple line).

S2.3. Infrared spectroscopy.

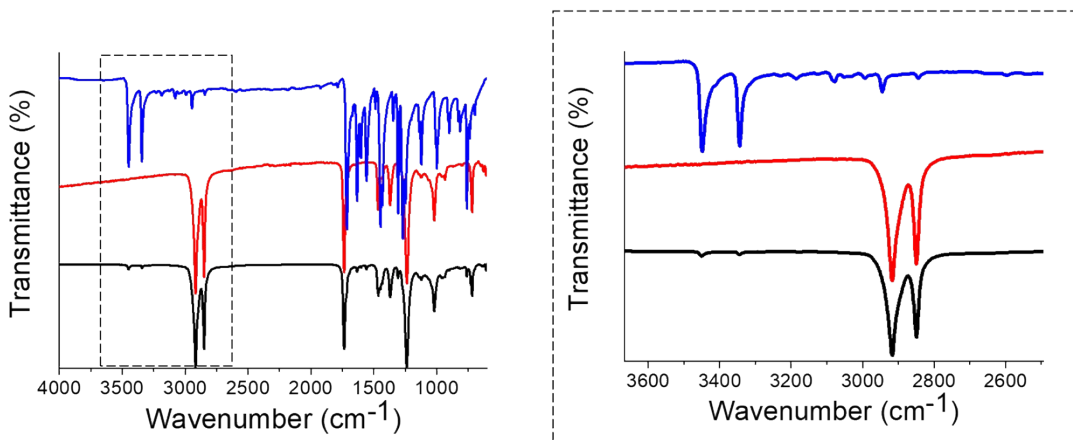


Figure S4. IR Spectrum of compound **1D-[Cu(NH₂-MeIN)I]_n** (blue line), **EVA** (red line) and **[Cu(NH₂-MeIN)I]_n@EVA-5%** composite thin film (black line).

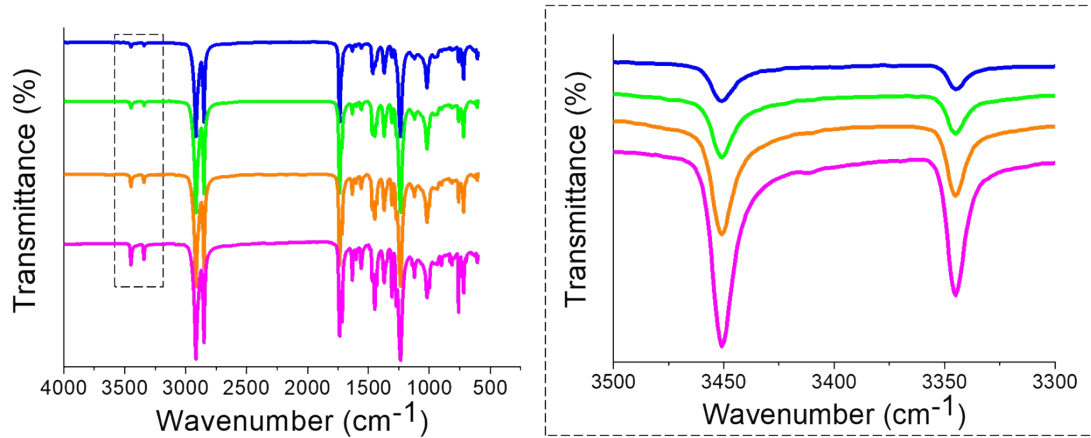
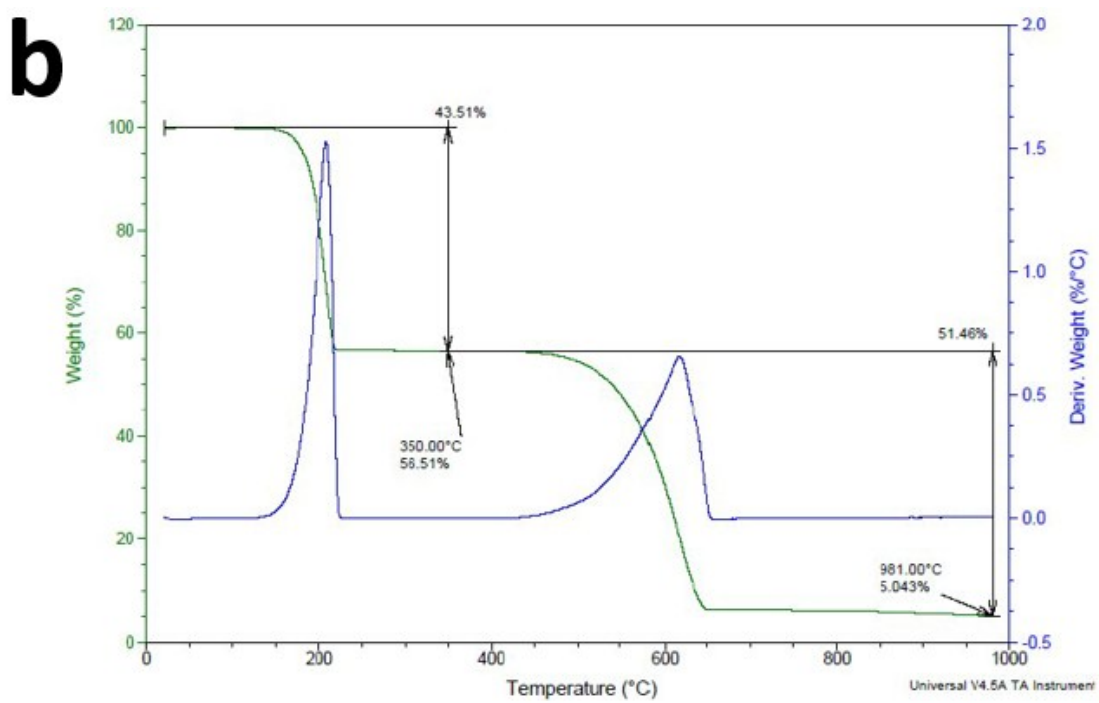
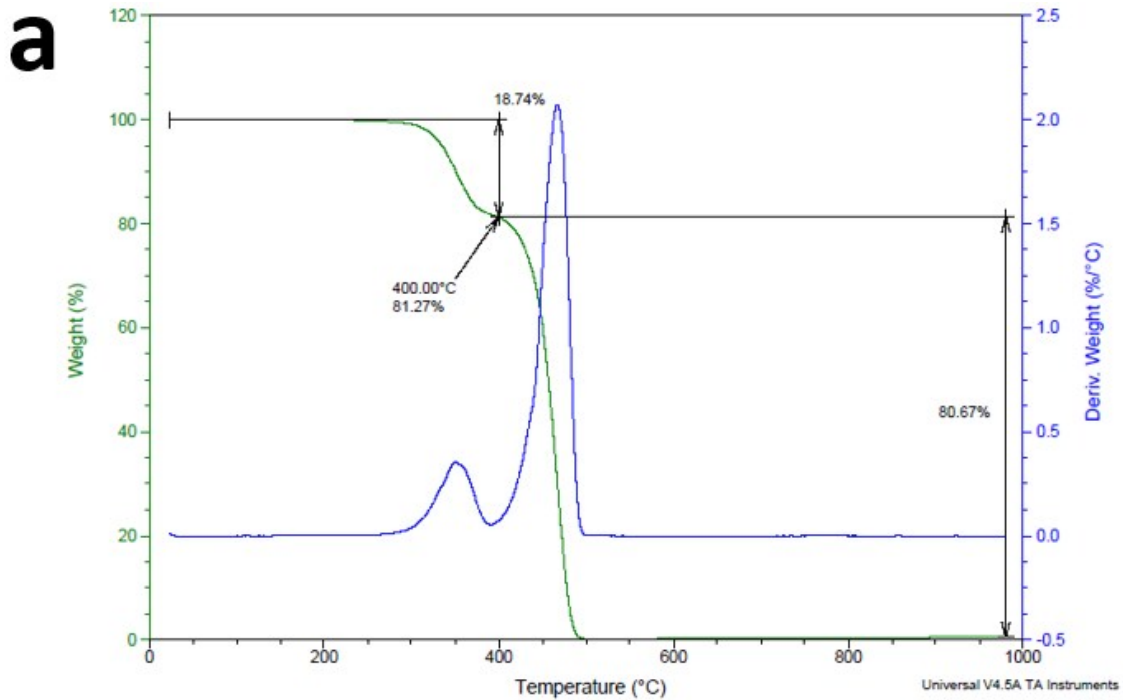
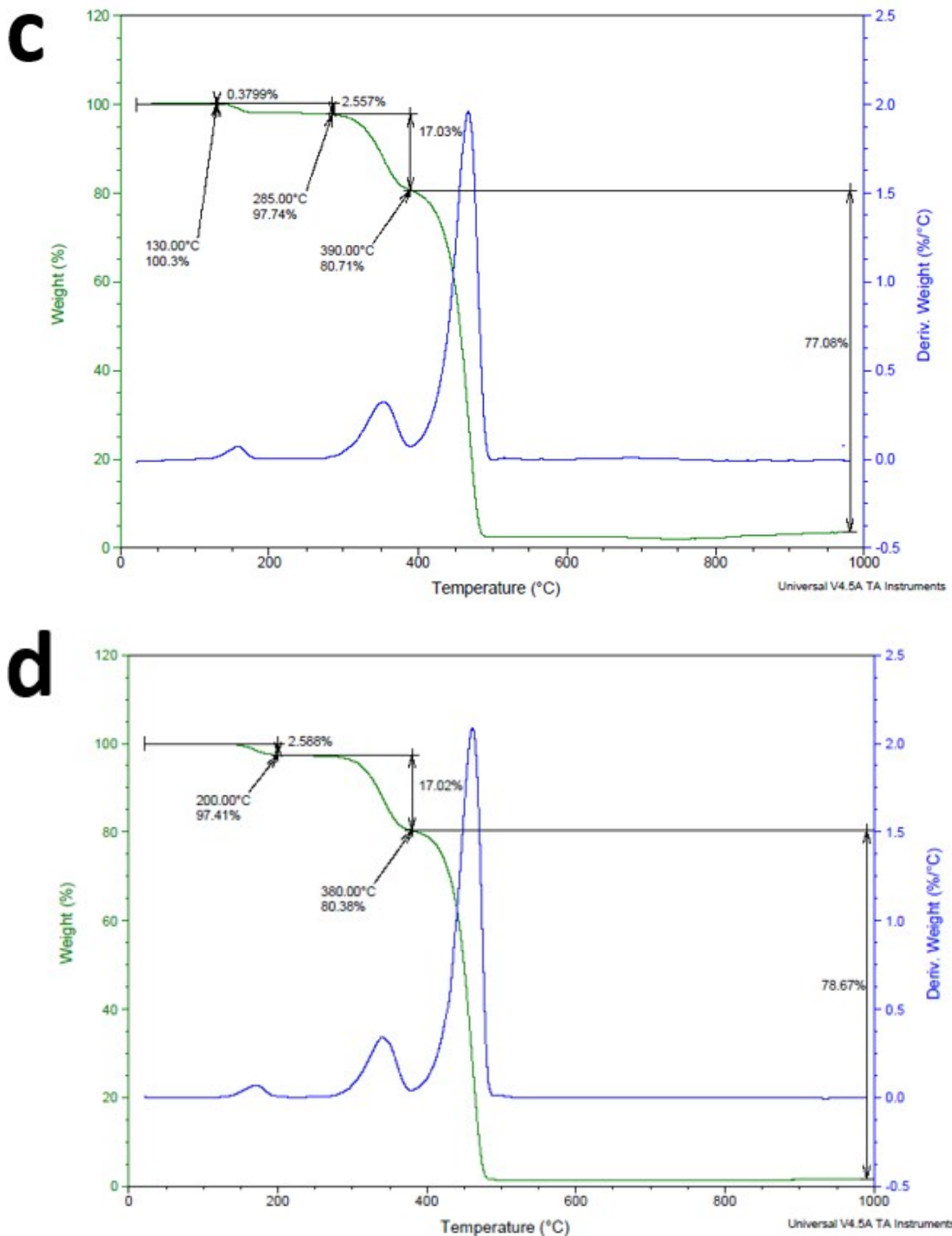


Figure S5. IR Spectrum of **[Cu(NH₂-MeIN)I]_n@EVA-5%** (blue line), **[Cu(NH₂-MeIN)I]_n@EVA-10%** (green line), **[Cu(NH₂-MeIN)I]_n@EVA-15%** (orange line) and **[Cu(NH₂-MeIN)I]_n@EVA-30%** (purple line) composite thin film.

S2.4. Thermal characterization.





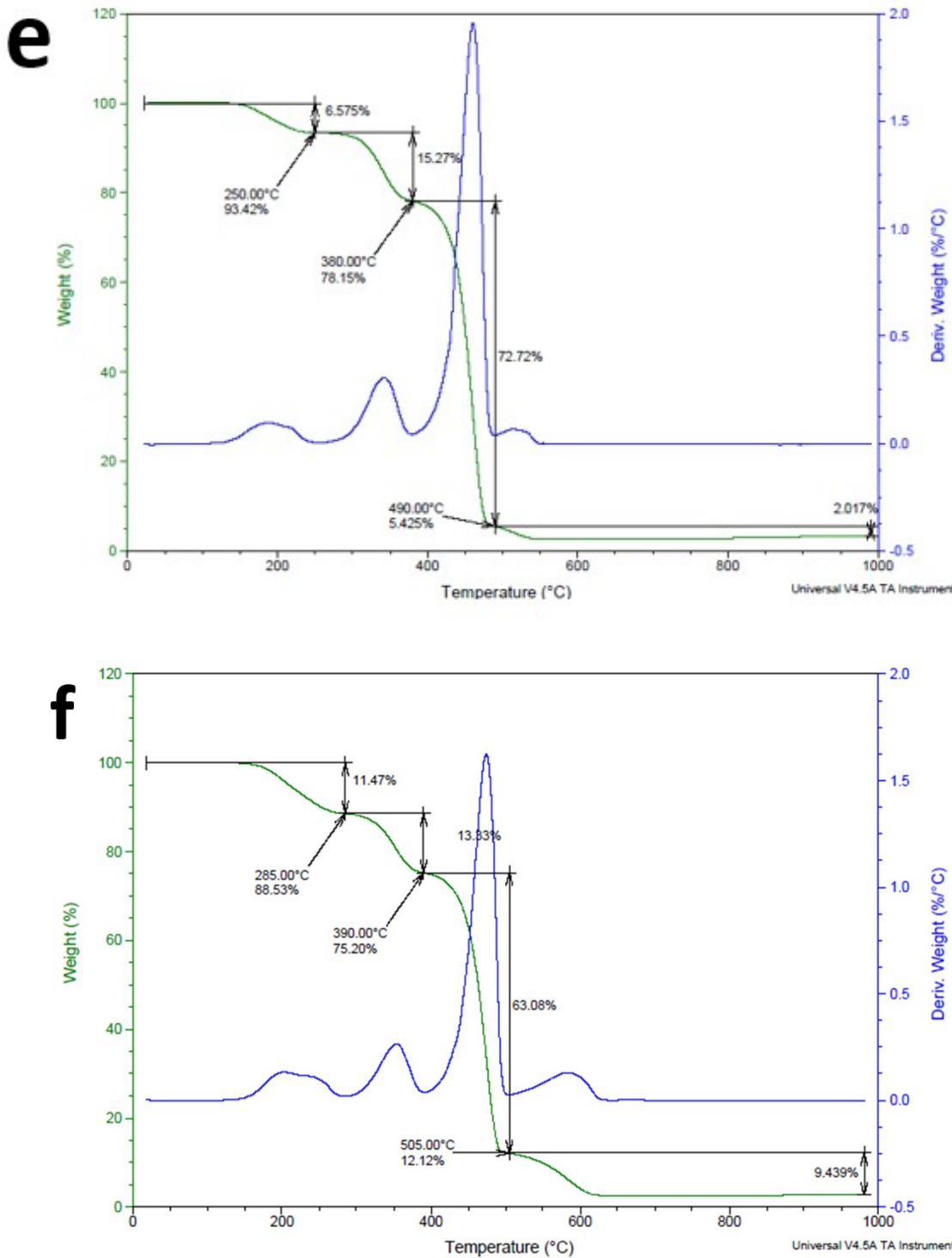


Figure S6. Thermogravimetric analysis coupled to differential thermal analysis (TGA-DTA) of a) EVA, b) 1D-[Cu(NH₂-MeIN)I]_n, c) [Cu(NH₂-MeIN)I]_n@EVA-5%, d) [Cu(NH₂-MeIN)I]_n@EVA-10%, e) [Cu(NH₂-MeIN)I]_n@EVA-15% and f) [Cu(NH₂-MeIN)I]_n@EVA-30% in a temperature range from 25 to 1000 °C, under nitrogen gas with flow rate of 90 mL/min and heating rate of 10 °C/min, in a range temperature from 25 to 1000 °C.

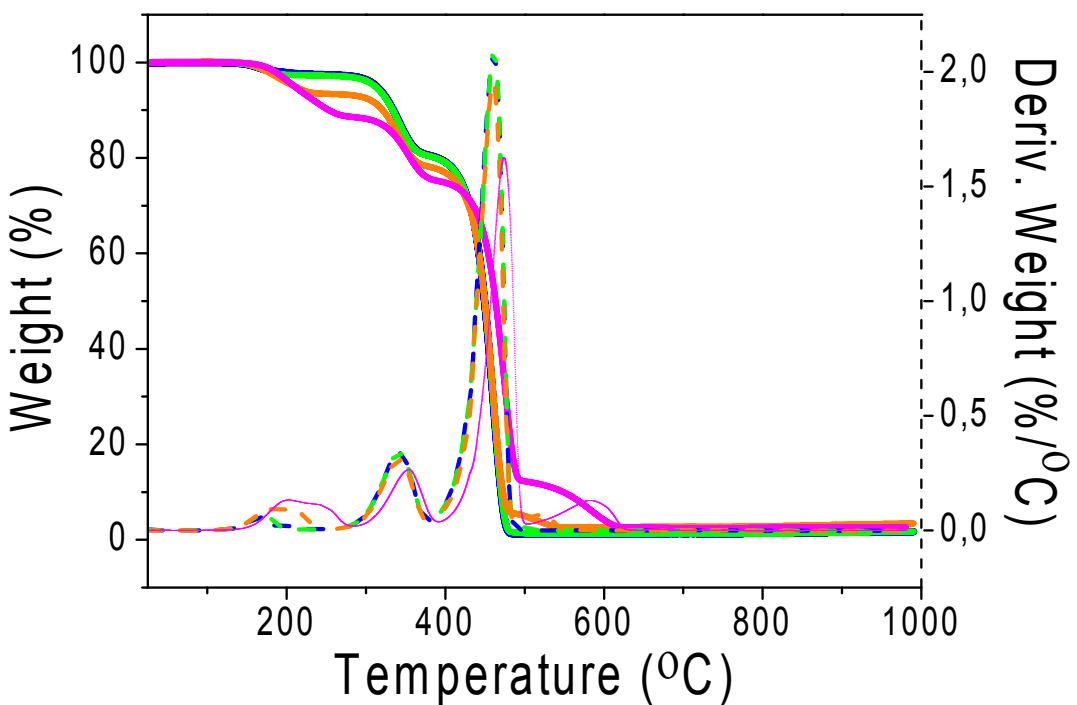


Figure S7. Thermogravimetric analysis coupled to differential thermal analysis (TGA-DTA) of $[\text{Cu}(\text{NH}_2\text{-MeIN})\text{I}]_n$ @EVA-5% (orange line) $[\text{Cu}(\text{NH}_2\text{-MeIN})\text{I}]_n$ @EVA-10% (green line), $[\text{Cu}(\text{NH}_2\text{-MeIN})\text{I}]_n$ @EVA-15% (blue line) and $[\text{Cu}(\text{NH}_2\text{-MeIN})\text{I}]_n$ @EVA-30% (purple line), thin films in a temperature range from 25 to 1000 °C, under nitrogen gas with flow rate of 90 mL/min and heating rate of 10 °C/min.

Table S3. Decomposition temperatures, maximum loss weights and residual weights of **1D- $[\text{Cu}(\text{NH}_2\text{-MeIN})\text{I}]_n$, EVA** and the composites $[\text{Cu}(\text{NH}_2\text{-MeIN})\text{I}]_n$ @EVA with different amounts of **1D- $[\text{Cu}(\text{NH}_2\text{-MeIN})\text{I}]_n$** .

Sample	T _{5%} (°C)	T _{max} (°C)	D _{max} (%/°C)	W _R (%)
1D- $[\text{Cu}(\text{NH}_2\text{-MeIN})\text{I}]_n$	181	209	1.528	5.040
EVA	335	467	2.081	0.599
$[\text{Cu}(\text{NH}_2\text{-MeIN})\text{I}]_n$ @EVA-5%	326	461	2.074	1.658
$[\text{Cu}(\text{NH}_2\text{-MeIN})\text{I}]_n$ @EVA-10%	311	461	2.092	1.717
$[\text{Cu}(\text{NH}_2\text{-MeIN})\text{I}]_n$ @EVA-15%	210	461	1.960	3.408
$[\text{Cu}(\text{NH}_2\text{-MeIN})\text{I}]_n$ @EVA-30%	210	474	1.626	2.682

S2.5. Diffuse reflectance UV-visible spectroscopy.

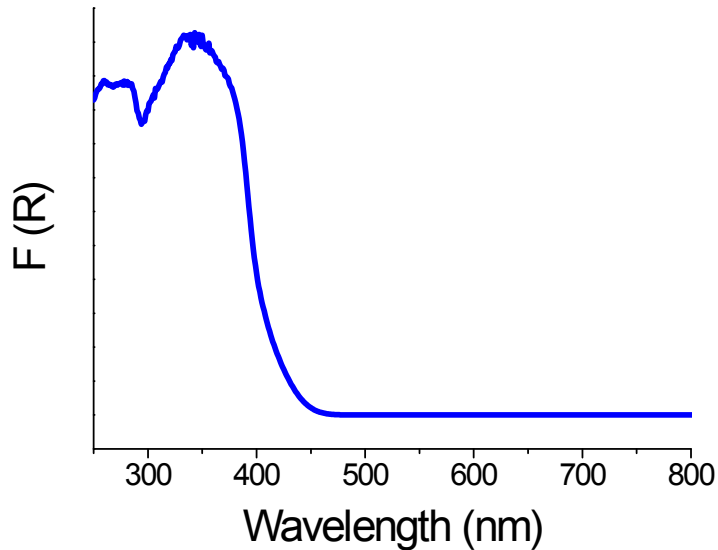


Figure S8. UV-visible spectrum of nano $1D\text{-}[Cu(NH_2\text{-MeIN})I]_n$ in solid state at 296K.

S3. Morphological studies.

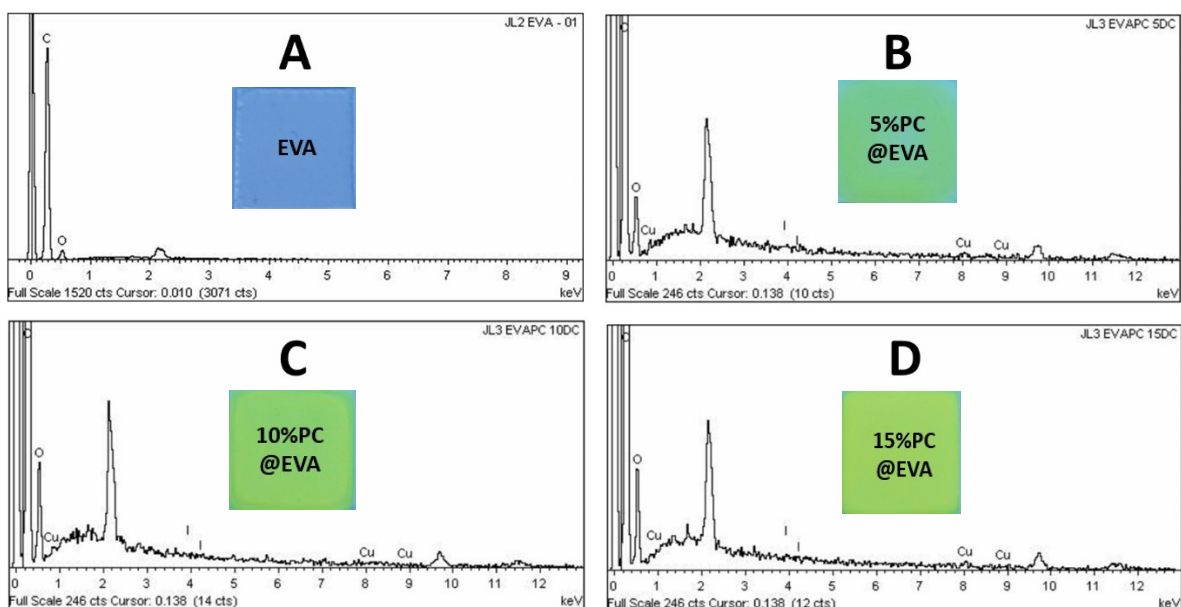


Figure S9. SEM-EDX analysis of: A. EVA. B. $[Cu(NH_2\text{-MeIN})I]_n\text{@EVA-5\%}$, C. $[Cu(NH_2\text{-MeIN})I]_n\text{@EVA-10\%}$, D. $[Cu(NH_2\text{-MeIN})I]_n\text{@EVA-15\%}$.

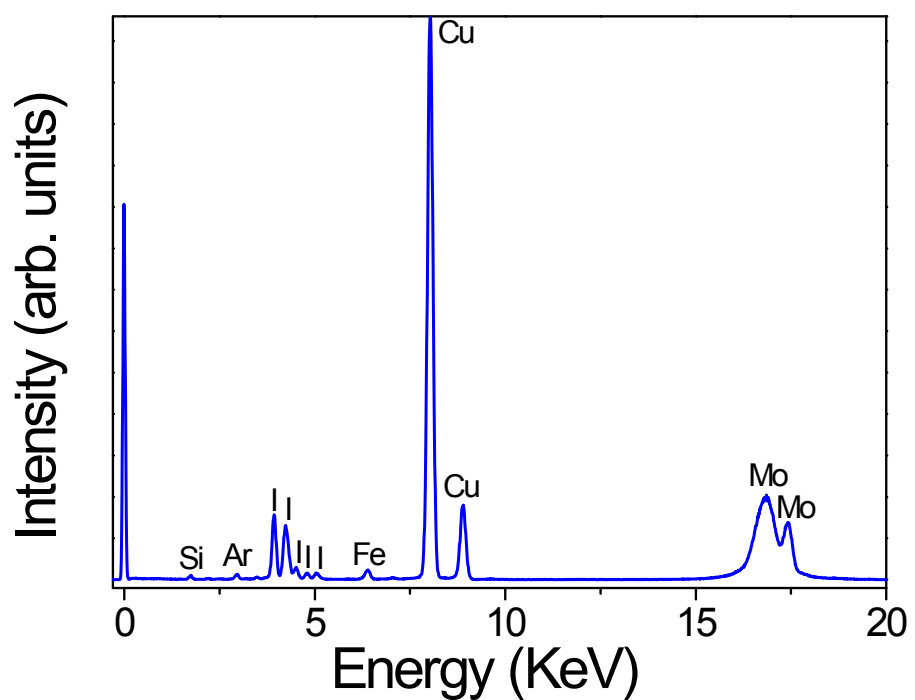


Figure S10. Qualitative spectra of $[\text{Cu}(\text{NH}_2\text{-MeIN})\text{I}]_n@\text{EVA-5\%}$ TXRF elemental profile for Mo- K_α X-ray excitation.

S3. Luminescent behavior.

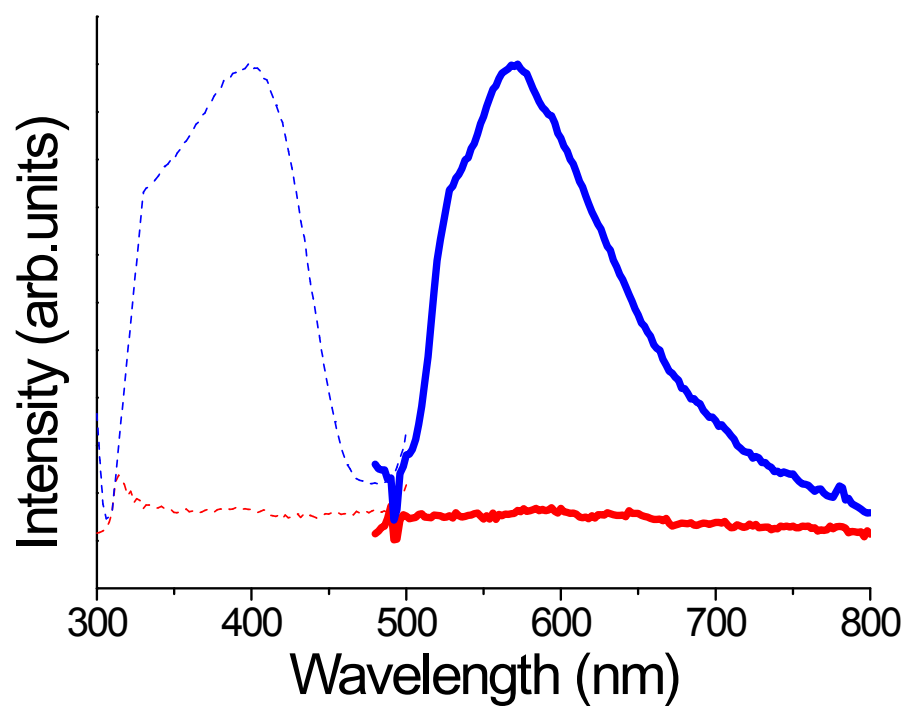


Figure S11. Excitation spectra (dashed lines, $\lambda_{\text{emi}}=570$ nm) and emission spectra (solid lines, $\lambda_{\text{exc}}=400$ nm) of $[\text{Cu}(\text{NH}_2\text{-MeIN})\text{I}]_n@\text{EVA-5\%}$ at 80 K (blue lines) and 300K (red lines).

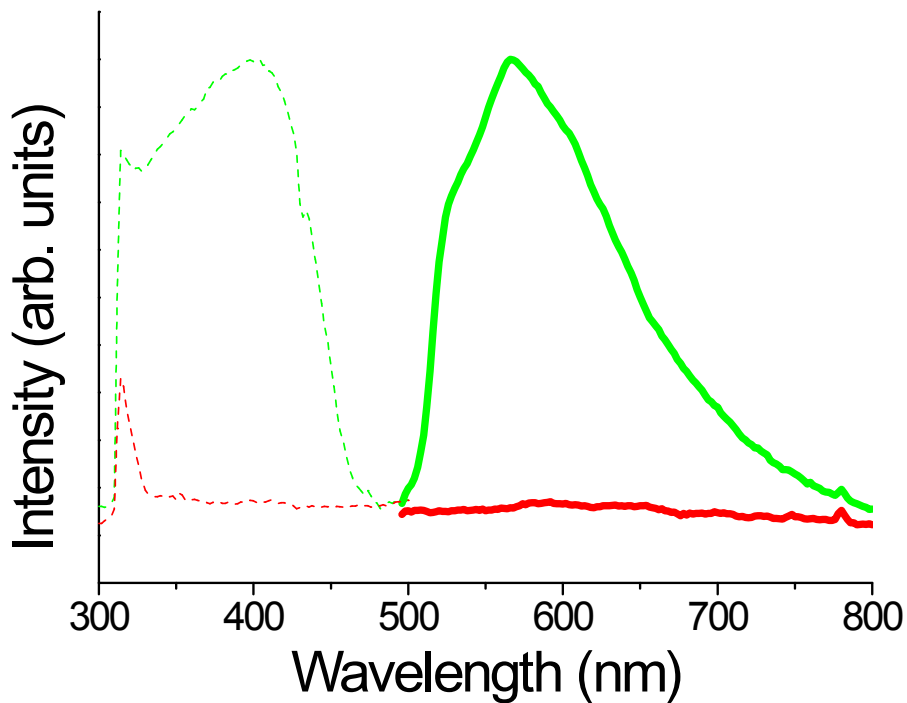


Figure S12. Excitation spectra (dashed lines, $\lambda_{\text{emi}}=570$ nm) and emission spectra (solid lines, $\lambda_{\text{exc}}=400$ nm) of $[\text{Cu}(\text{NH}_2\text{-MeIN})\text{I}]_n@\text{EVA-10\%}$ at 80 K (green lines) and 300K (red lines).

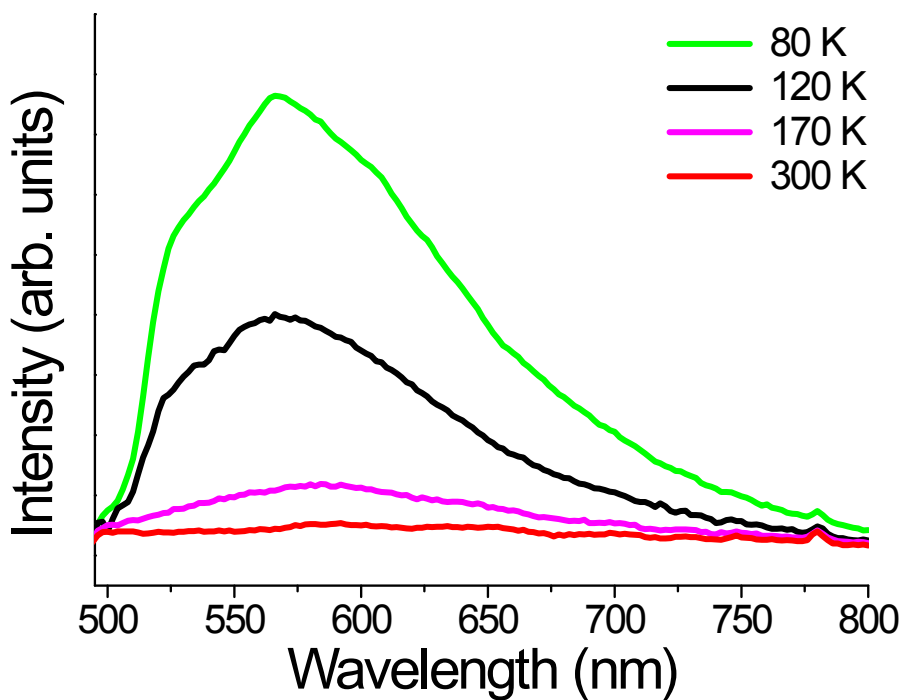


Figure S13. Temperature-dependence of the luminescence spectra of $[\text{Cu}(\text{NH}_2\text{-MeIN})\text{I}]_n@\text{EVA-10\%}$ ($\lambda_{\text{exc}}=400$ nm) from 300 to 80 K.

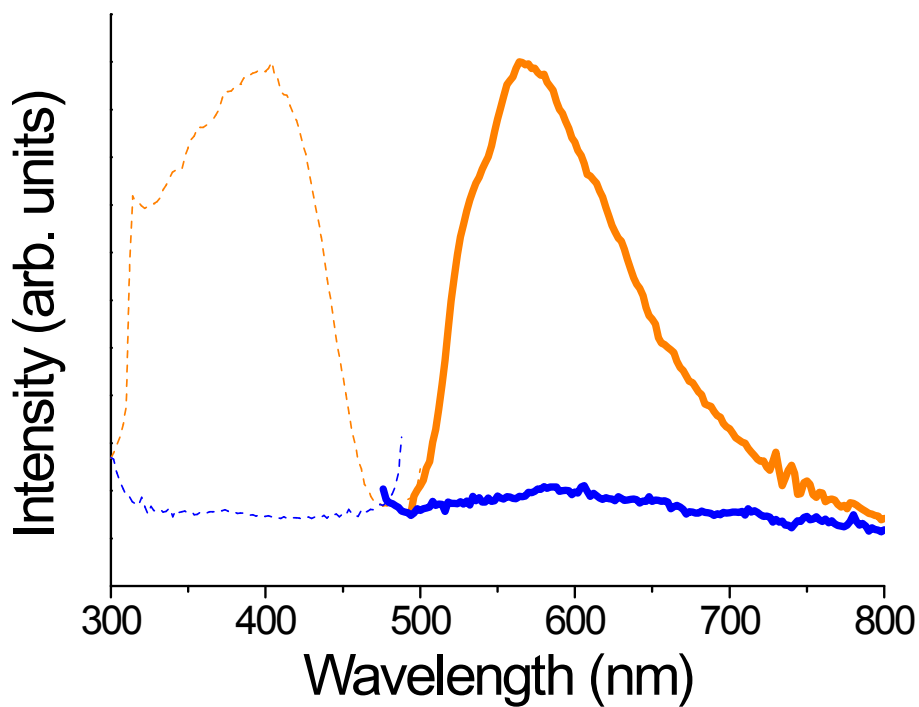


Figure S14. Excitation spectra (dashed lines, $\lambda_{\text{emi}} = 570 \text{ nm}$) and emission spectra (solid lines, $\lambda_{\text{exc}} = 400 \text{ nm}$) of $[\text{Cu}(\text{NH}_2\text{-MeIN})\text{I}]_n$ @EVA-15% at 80 K (orange lines) and 300K (blue lines).

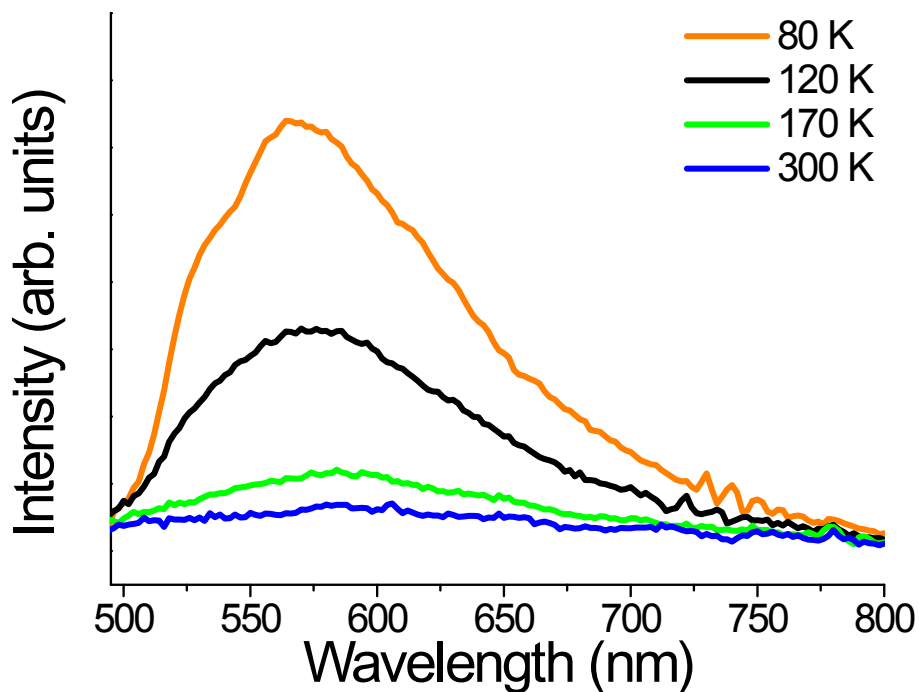


Figure S15 Temperature-dependence of the luminescence spectra of $[\text{Cu}(\text{NH}_2\text{-MeIN})\text{I}]_n$ @EVA-15% ($\lambda_{\text{exc}} = 400 \text{ nm}$) from 300 to 80 K.

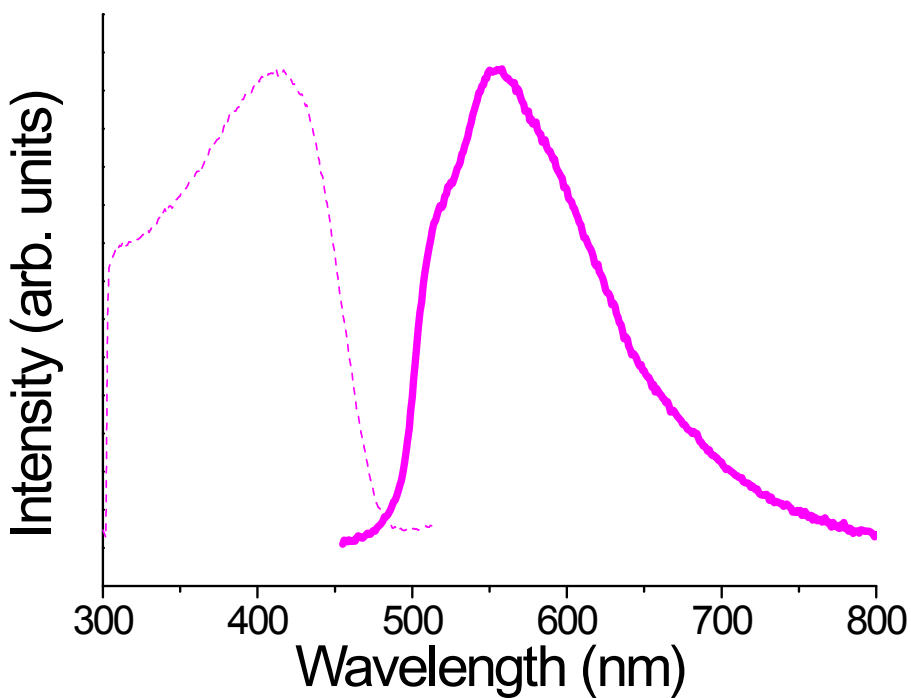


Figure S16. Excitation spectra (dashed lines, $\lambda_{\text{emi}} = 570 \text{ nm}$) and emission spectra (solid lines, $\lambda_{\text{exc}} = 400 \text{ nm}$) of $[\text{Cu}(\text{NH}_2\text{-MeIN})\text{I}]_n$ @EVA-30% at 80 K (purple lines).

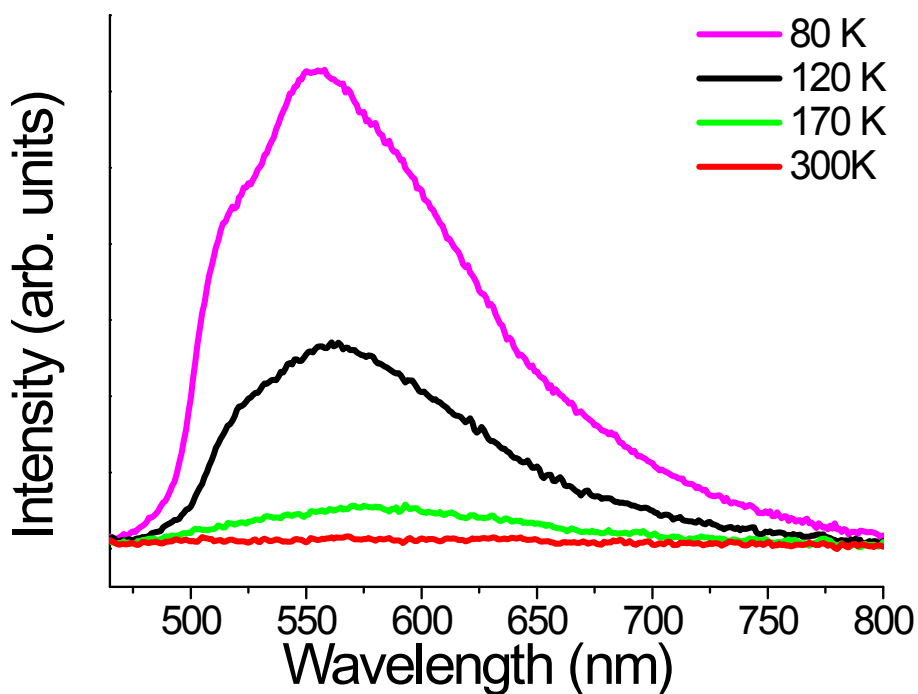


Figure S17. Temperature-dependence of the luminescence spectra of $[\text{Cu}(\text{NH}_2\text{-MeIN})\text{I}]_n$ @EVA-30% ($\lambda_{\text{exc}} = 400 \text{ nm}$) from 300 to 80 K.

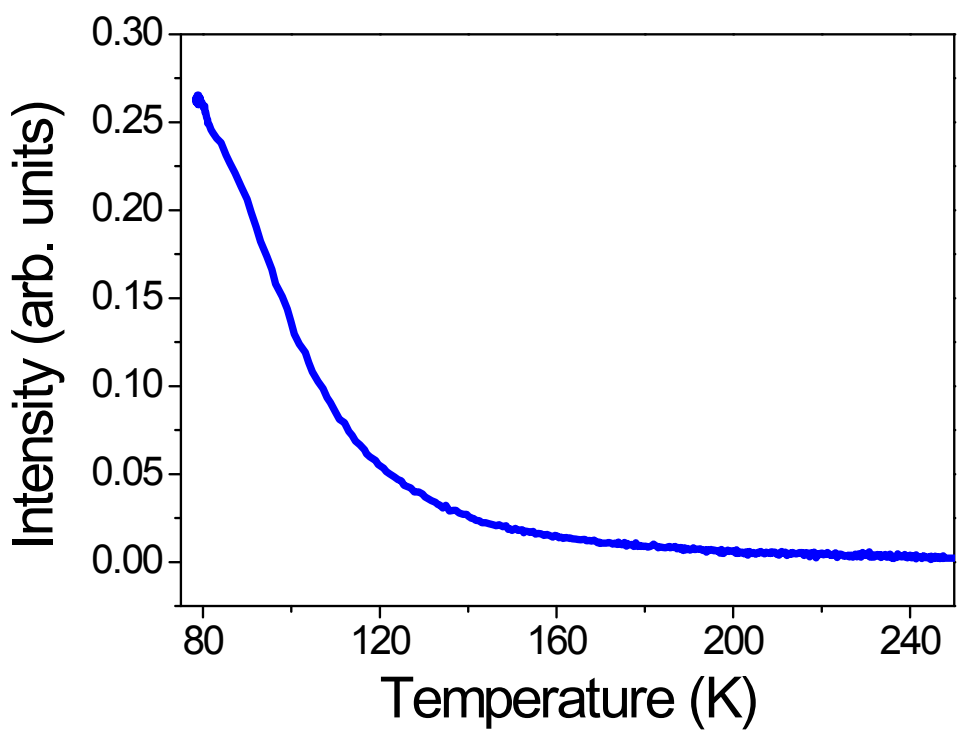


Figure S18 Temperature-dependence emission intensity of $[\text{Cu}(\text{NH}_2\text{-MeIN})\text{I}]_n$ @EVA-5% from 80 to 300 K ($\lambda_{\text{exc}}=400 \text{ nm}$, $\lambda_{\text{emi}}=570 \text{ nm}$).

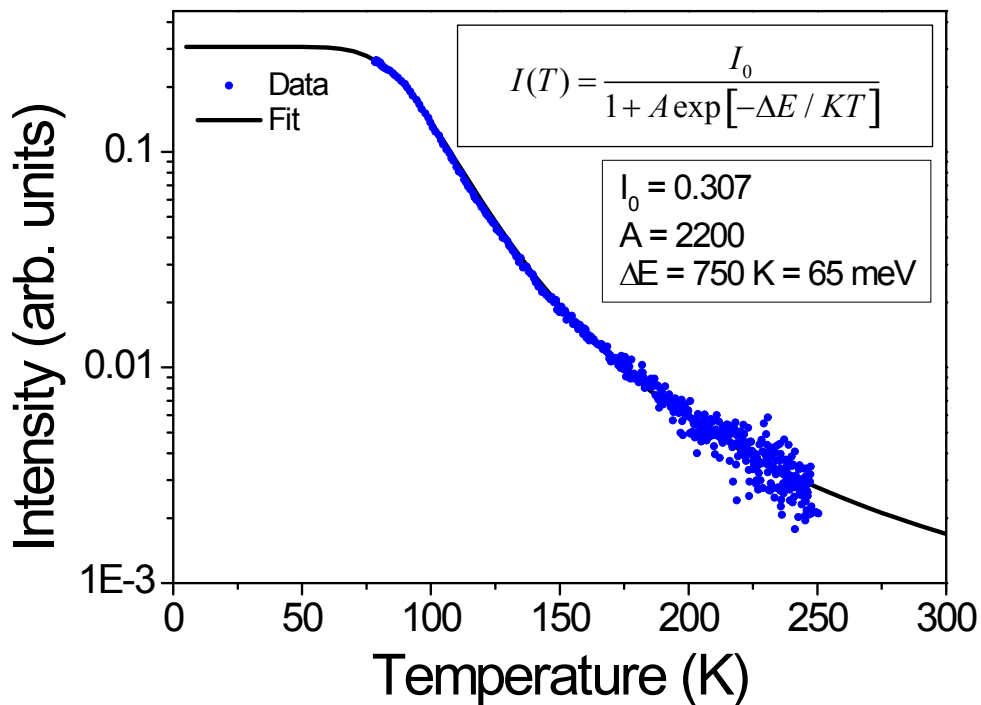


Figure S19. Logarithm plot of the intensity as function of the temperature of $[\text{Cu}(\text{NH}_2\text{-MeIN})\text{I}]_n$ @EVA-5% from 80 to 300 K ($\lambda_{\text{exc}}=400 \text{ nm}$, $\lambda_{\text{emi}}=570 \text{ nm}$). Circles: experimental data. Line: fit of the data according to the formula in the graph. The inset shows the fitted parameters.

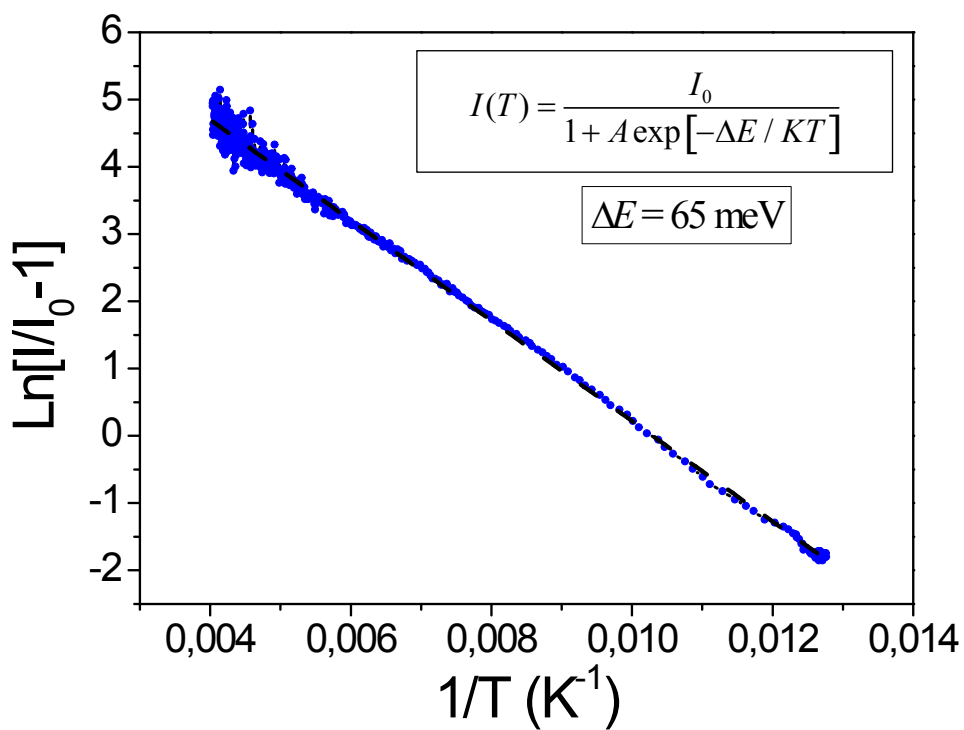


Figure S20. Graph of $\ln(I/I_0 - 1)$ vs inverse of the temperature of $[\text{Cu}(\text{NH}_2\text{-MeIN})\text{I}]_n@\text{EVA-5\%}$ from 80 to 300 K ($\lambda_{\text{exc}} = 400 \text{ nm}$, $\lambda_{\text{emi}} = 570 \text{ nm}$). The dashed line corresponds to the formula in the graph, which give an activation energy of 65 meV.

S5. Transparency and flexibility of $[\text{Cu}(\text{NH}_2\text{-MeIN})\text{I}]_n@\text{EVA}$ thin films.

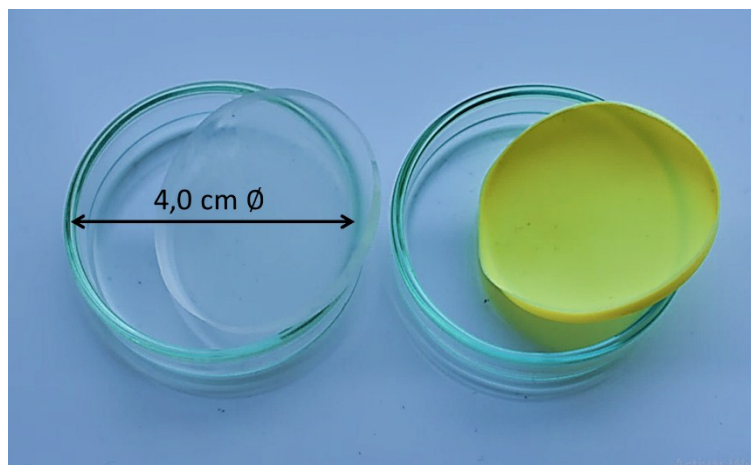


Figure S21. Transparency degree in a naked eye experiment under white light at 296K of EVA (left) and $[\text{Cu}(\text{NH}_2\text{-MeIN})\text{I}]_n@\text{EVA-30\%}$ thin films (right).

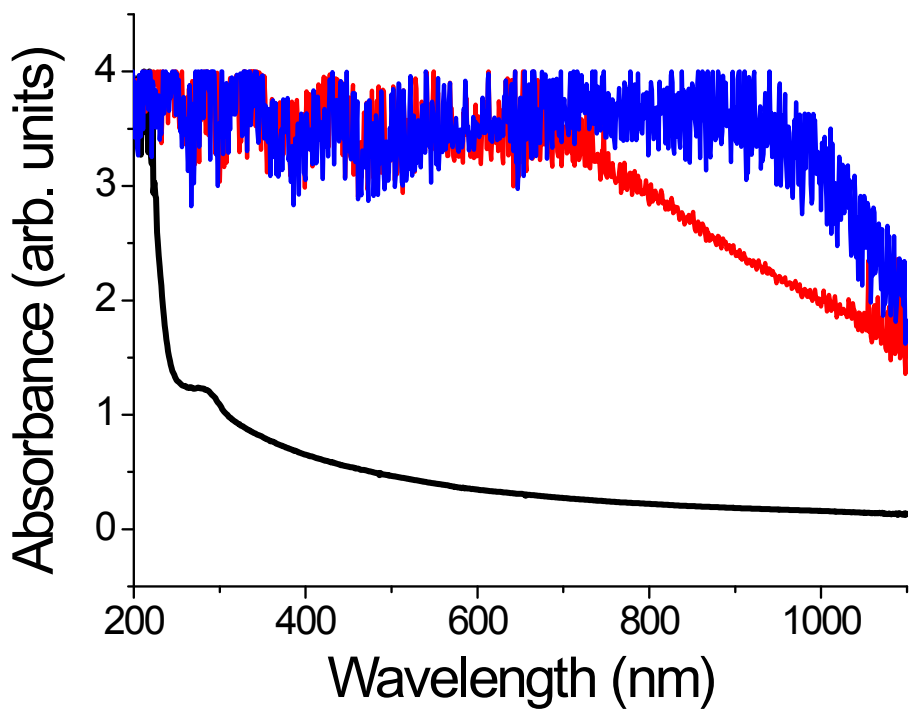
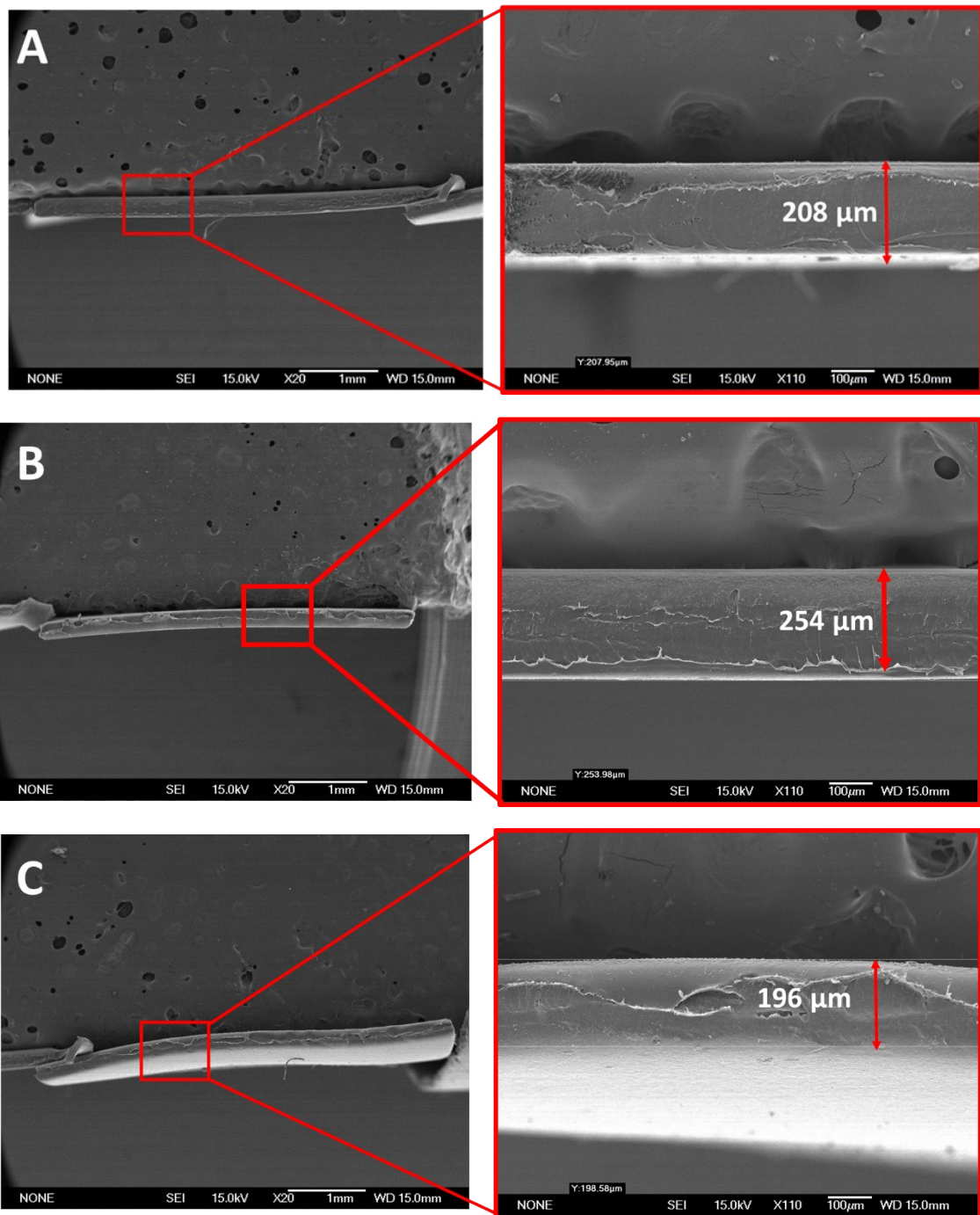


Figure S22. UV/Visible absorbance spectrum of EVA (black line), $[\text{Cu}(\text{NH}_2\text{-MeIN})\text{I}]_n@\text{EVA-5\%}$ (red line) and $[\text{Cu}(\text{NH}_2\text{-MeIN})\text{I}]_n@\text{EVA-10\%}$ (blue line), in a wavelength range from 200 to 1000 nm at 296K.

S6. SEM study.



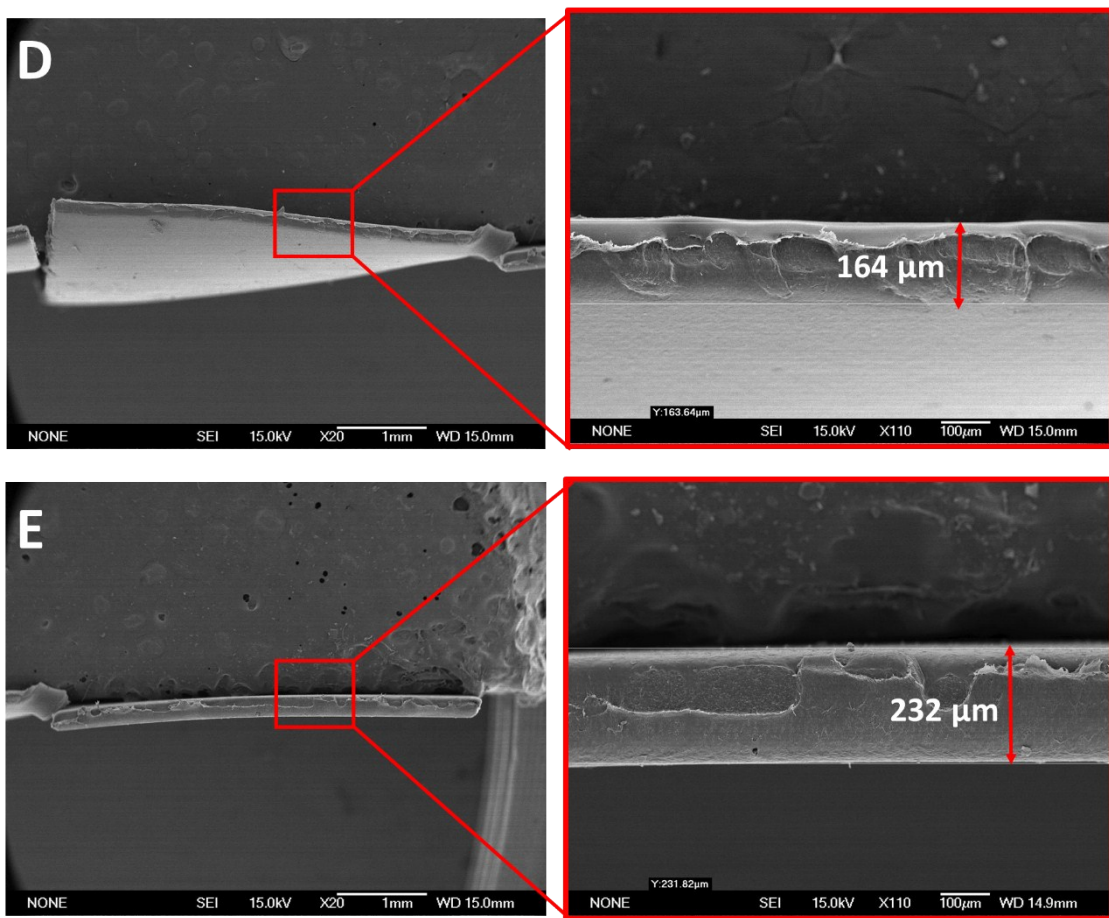
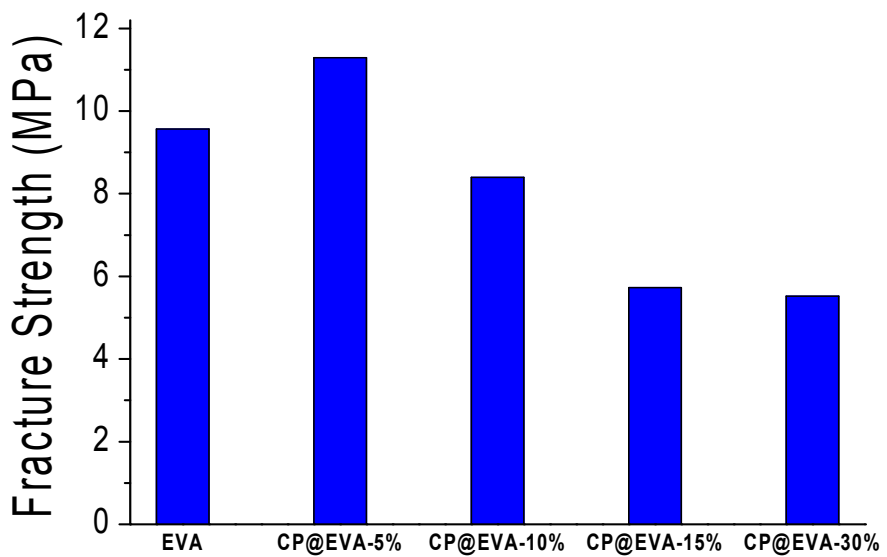
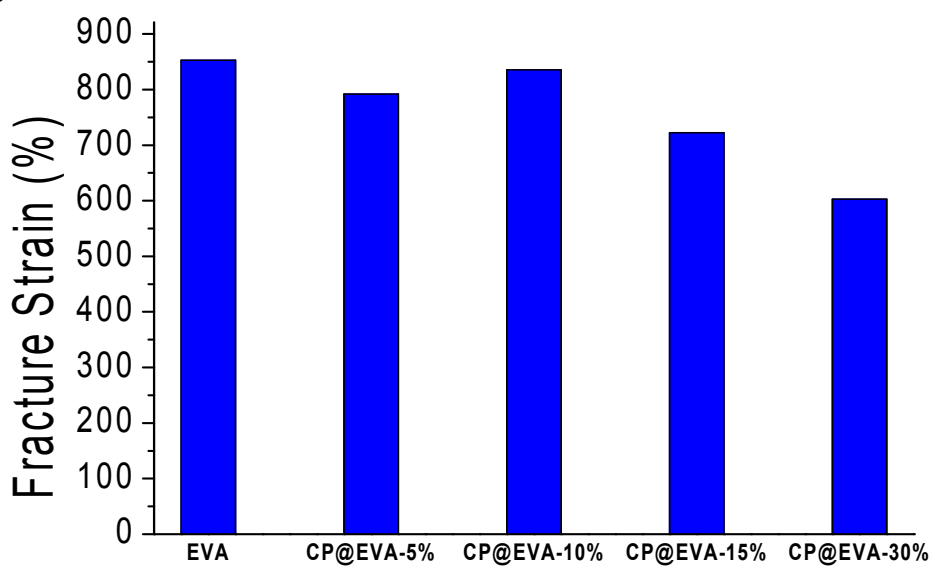


Figure S23. SEM images of the edges of EVA (A), $[\text{Cu}(\text{NH}_2\text{-MeIN})\text{I}]_n@\text{EVA-5\%}$ (B), $[\text{Cu}(\text{NH}_2\text{-MeIN})\text{I}]_n@\text{EVA-10\%}$ (C), $[\text{Cu}(\text{NH}_2\text{-MeIN})\text{I}]_n@\text{EVA-15\%}$ (D) and $[\text{Cu}(\text{NH}_2\text{-MeIN})\text{I}]_n@\text{EVA-30\%}$ (E) films prepared by drop-casting.

S7. Stress-Strain curves



Figure S24. Macrograph of $[\text{Cu}(\text{NH}_2\text{-MeIN})\text{I}]_n@\text{EVA}$ composite sample.

A**B**

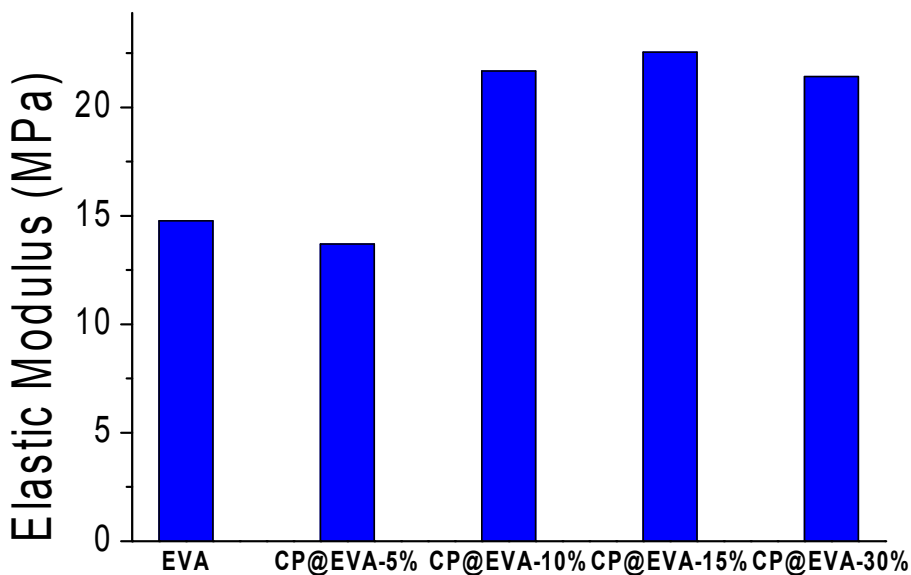
C

Figure S26: Fracture strength (σ_u) (A), fracture strain (e_f) (B) and elastic modulus E (C) for EVA and $[\text{Cu}(\text{NH}_2\text{-MeIN})\text{I}]_n$ @EVA composites.

Table S4: Mean value and standard deviation of EVA and $[\text{Cu}(\text{NH}_2\text{-MeIN})\text{I}]_n$ @EVA composites.

	σ_u (MPa)	e_f (%)	E (MPa)
EVA	9.56±0.38	852.9±36.1	14.77± 3.39
CP@EVA-5%	11.29±0.99	792.0±15.1	13.70± 5.26
CP@EVA-10%	8.39±0.39	835.3±19.7	21.68± 3.28
CP@EVA-15%	5.72±0.08	722.1±6.3	22.55± 8.01
CP@EVA-30%	5.51±0.68	602.7±87.7	21.42± 6.42

Fracture strength (σ_u) for EVA matrix is ranged from 9.02 MPa to 9.87 MPa, with a mean value of 9.56 MPa and standard deviation of 0.38 MPa. Maximum and minimum values for fracture strain (e_f) differ from 803.6% to 889.4%. These values are grouped closely having a mean value of strain of 852.9% and variance of 36.1%. These values are in agreement with the data in the literature (CESedupack). Meanwhile, in the case of elastic modulus E, the mean value reaches 14.77 MPa and the standard deviation 3.39 MPa having a maximum Young modulus of 18.52 and a minimum of 10.28 MPa.